Biosensors and Bioelectronics 142 (2019) 111487

Contents lists available at ScienceDirect

Biosensors and Bioelectronics

journal homepage: www.elsevier.com/locate/bios

A visible light photoelectrochemical sandwich aptasensor for adenosine triphosphate based on $MgIn_2S_4$-TiO_2 nanoarray heterojunction

Liwei Yang[a], Xiaoqiang Liu[a,**], Lele Li[a], Si Zhang[a], Hejie Zheng[a], Yunfei Tang[a], Huangxian Ju[b,*]

[a] Henan Joint International Research Laboratory of Environmental Pollution Control Materials, College of Chemistry and Chemical Engineering, Henan University, Kaifeng, 475004, PR China

[b] State Key Laboratory of Analytical Chemistry for Life Science, College of Chemistry and Chemical Engineering, Nanjing University, Nanjing, 210023, PR China

ARTICLE INFO

Keywords:
Photoelectrochemical sensing
Sandwich aptasensor
Heterojunction
TiO_2 nanoarray
$MgIn_2S_4$ nanoplate
Adenosine triphosphate

ABSTRACT

This work designed a $MgIn_2S_4$-TiONA heterojunction by growing $MgIn_2S_4$ nanoplates on TiO_2 nanowire array (TiONA) for preparation of visible light photoelectrochemical (PEC) sensing platform. The heterojunction exhibited strong absorption of visible light, large surface area and high loading of biomolecules, leading to high sensing sensitivity. Using adenosine triphosphate (ATP), a marker of cell vitality, as the target model, a PEC sandwich aptasensor was constructed by immobilizing capture DNA_1 on $MgIn_2S_4$ surface. In the presence of ATP and signal DNA_2 with terminal ferrocene as the electron donor, a sandwiched DNA_1-ATP-DNA_2 complex could be formed on the PEC aptasensor. The aptasensor showed excellent performance with a wide linear range from 50 fM to 100 nM and a detection limit of 20 fM. The sensing performance including specificity, reproducibility, stability and practical use were also evaluated, showing promising application of the $MgIn_2S_4$-TiONA heterojunction in PEC biosensing.

1. Introduction

As the 'energy currency of life', adenosine triphosphate (ATP) provides the most direct source of energy for the living cell and plays a vital role in the organism (Deng et al., 2017). In addition, ATP concentration in metabolically active cells decreases abruptly when the cells suffer necrosis or apoptosis, making ATP a typical marker for cellular vitality (Verstraeten et al., 1983). Accordingly, some sickness including angiocardiopathy (Yokoshiki et al., 1998), malignant tumors, hypoglycemia and Parkinson's disease can be detected through the accurate measuring of ATP level (Lu et al., 2015; Zhou et al., 2016). Various techniques including colorimetric (Huo et al., 2016b; Wang et al., 2007), fluorescent (Xu and Lu, 2010), chemiluminescent (Zhou et al., 2016), electrochemical (Kashefi-Kheyrabadi and Mehrgardi, 2012; Shahdost-fard et al., 2014; Shahdost-fard et al., 2013; Wang et al., 2018b; Wu et al., 2015; Zuo et al., 2009) and electrochemiluminescent (Lu et al., 2013) methods have been explored to detect ATP in recent years. Nonetheless, it is still meaningful to develop a simple, fast and sensitive strategy for ATP detection because of the extreme importance of ATP in clinical diagnosis and biochemical research.

Photoelectrochemical (PEC) biosensors, consisting of photoactive semiconductors and biorecognition components, have widely been used in drug, biomolecular and environmental analysis (Cao et al., 2015; Liu et al., 2017d, 2018; Tang et al., 2018) due to their simple equipment, less running time, low cost and easy procedures. In addition, low background signal can also be achieved at PEC biosensor owing to the complete separation of the excitation source with the detection signal. By using aptamers as the recognition components, the developed PEC sensors have been endowed with good selectivity (Dong et al., 2017; Huo et al., 2016a; Liu et al., 2017a; Ranjbar et al., 2018). However, the sensitivity of the PEC aptasensor has not shown significant superiority over those of the electrochemical biosensors (Deng et al., 2019; Xia et al., 2017a, 2017b). Therefore, the nanomaterials with super-duper photoelectric activity as biosensor scaffolds are highly demanded to improve the performance of PEC biosensors, which is also the focus and difficulty of this research field.

Lately, ternary chalcogenide AB_2X_4 materials have exhibited incredible photocatalytic activity under visible light because of their tunable optical properties, proper band gap and band edge. However, the severe agglomeration, photo-etching under light irradiation and high hole-electron recombination rate limit their applications (Chen et al., 2017b). The heterojunction of AB_2X_4 with other proper materials can effectively minimize the disadvantages (Jiang et al., 2015; Yu et al.,

* Corresponding author.
** Corresponding author.
E-mail addresses: liuxq@henu.edu.cn (X. Liu), hxju@nju.edu.cn (H. Ju).

https://doi.org/10.1016/j.bios.2019.111487
Received 18 April 2019; Received in revised form 16 June 2019; Accepted 29 June 2019
Available online 29 June 2019
0956-5663/

2013) because of its high photo-generated charge separation and strong anti-photocorrosion. TiO_2 nanomaterials have been used as good candidates to combine with AB_2X_4 due to their photostability, controllable morphology and large surface area (Wang et al., 2018a; Yoon et al., 2001; Zhao et al., 2014). Especially, as a one-dimensional nanostructure, TiO_2 nanowire array (TiONA) displays some excellent photoelectric properties such as smaller bandgap (~3.0 eV), higher electrical conductivity and lower electron-hole recombination rate than TiO_2 nanoparticles (~3.2 eV) (Feng et al., 2008; Wang et al., 2011). For example, a maximum light conversion efficiency of 2.25% (100 mW/cm^2 AM 1.5 global illumination) has been achieved at TiONA compared with that of 1.9% at a anatase/rutile TiO_2 nanoparticle thin film (Murphy et al., 2006). Therefore, this work used TiONA to construct a $MgIn_2S_4$-TiONA heterojunction for improving the light conversion efficiency, which led to a high sensitive visible light PEC sensing platform.

The $MgIn_2S_4$-TiONA heterojunction was prepared by growing $MgIn_2S_4$ nanoplates on TiONA modified FTO electrode using a hydrothermal method. The TiONA provided a large surface for loading of $MgIn_2S_4$ nanoplates and minimized their agglomeration. The well-dispersive $MgIn_2S_4$-TiONA was then carboxylated by assembling 3-mercaptopropionic acid on its surface for capturing aptamer sequence DNA_1. After successive immobilization of ATP and signal DNA_2 with terminal ferrocene (DNA_2-Fc), a DNA_1-ATP-DNA_2 sandwich structure was formed on the heterojunction for PEC biosensing (Scheme 1). Herein, ferrocene at the end of DNA_2 acted as an electron donor, which could increase the photocurrent and amplify the signal. In addition, the sandwich structure led to higher specificity and sensitivity than those with competitive structure. The PEC aptasensor showed good repeatability for assay of ATP. These results indicated that the designed heterojunction was a promising candidate to fabricate PEC biosensors for different analytes.

2. Experimental

2.1. Material and reagents

Fluorine-doped tin oxide (FTO) glasses (5 mm × 40 mm × 1.6 mm, resistivity ~14 Ω) were obtained from Wuhan Lattice Solar Energy Technology, Ltd., China. Concentrated hydrochloric acid (37 wt%), magnesium nitrate hexahydrate and tetrabutyl titanate were booked from Tianjin Chemical Reagent Co., Ltd., China. Ultrapure water (≥18 MΩ cm^{-1}) was obtained from a Millipore water purification system and used throughout the whole experiment. L-cysteine (99%) and indium nitrate hydrate were bought from Sinopharm Chemical Reagent Co., Ltd. (Shanghai, China). Phosphate buffered saline (PBS, pH 7.4) was prepared with the stock solutions of 0.1 M KH_2PO_4, K_2HPO_4 and KCl. Adenosine triphosphate (ATP), cytidine triphosphate (CTP), guanosine triphosphate (GTP), uridine triphosphate (UTP) and bovine serum albumin (BSA) were purchased from Aladdin Chemistry Co. Ltd. DNA sequences were prepared by Shanghai Sangon Biotechnology Co. Ltd. (Shanghai, China).

DNA_1: 5′–NH_2–TTTTTTTTTTACCTGGGGGAGTAT-3′

DNA_2: 5′-TGCGGAGGAAGGTTTTTT-Ferrocene-3′

2.2. Apparatus

PEC measurements were conducted at room temperature with a conventional three-electrode system in a cell containing 0.1 M PBS solution. The modified FTO electrode was used as the working electrode, a platinum wire as the auxiliary electrode, and Ag|AgCl electrode (3.0 M KCl) as the reference electrode. The PEC detection system employed a Xe lamp equipped with a 400 nm cut-off filter as the visible light source (CEL-HXUV 300, Beijing AULTT, China), and a CHI630D electrochemical workstation as the detector (CH Instruments, Shanghai, China). Electrochemical impedance spectroscopic measurements were performed using an IM6ex electrochemical station (ZAHNER, Germany). The morphology and chemical composition of the materials were characterized with a field emission scanning electron microscopy (SEM, JSM-7500F, JEOL., Japan), a X-ray diffraction spectrometer (XRD, Bruker D8 Advance, Germany) with a Cu Kα radiation, and an X-ray photoelectron spectrometer (ESCALAB 250Xi, USA) with a monochromatic Al Kα source (hν = 1486.6 eV, 150 W power , 500 μm beam spot). The XPS spectra were calibrated on the C1s peak (284.8 eV) and analyzed by XPSPEAK41 software. UV − vis diffuse reflectance spectra of the samples were recorded on an UV − vis spectrophotometer (DRS, UV-2600, Kyoto, Japan).

2.3. Preparation of TiO_2 nanowire array

The rutile TiO_2 nanowire array was synthesized on FTO glass with a previously reported hydrothermal method. Initially, the FTO substrate

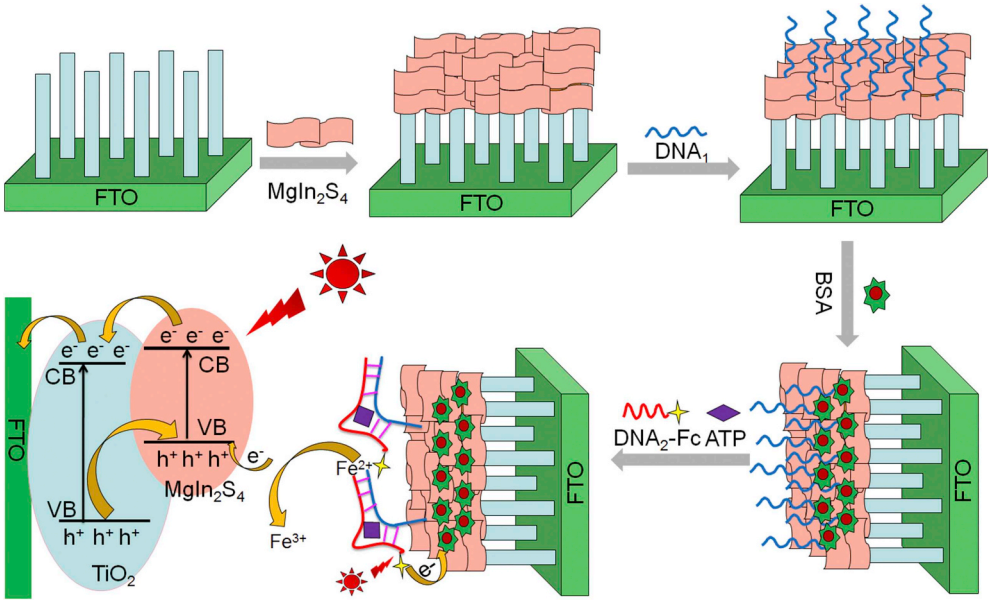

Scheme 1. Schematic diagram of preparation and PEC mechanism of the aptasensor.

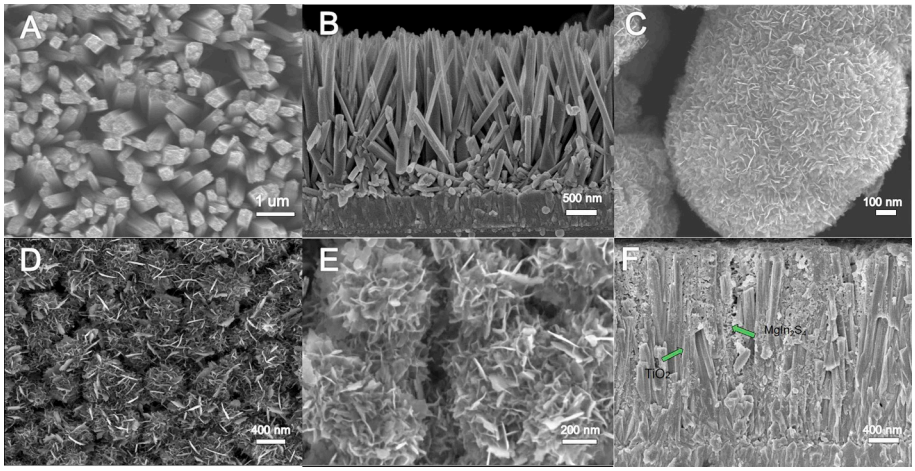

Fig. 1. SEM images of plan (A) and side (B) views of TiONA, (C) $MgIn_2S_4$ nanoplates, (D) and (E) $MgIn_2S_4$-TiONA at different magnifications, (F) side view of $MgIn_2S_4$-TiONA.

was successively washed with toluene, acetone, ethanol and ultrapure water, and dried under a N_2 stream. Afterward, 400 μL of tetrabutyl titanate was added in a solution containing 15 mL of concentrated HCl (37 wt%) and 15 mL of ultrapure water. The obtained dispersion solution was stirred for 30 min and then transferred to a 100 mL Teflon-lined stainless-steel autoclave. The cleaned FTO substrate was placed in the autoclave, which was sealed and heated at 160 °C for 12 h. Subsequently, a FTO substrate coated with a white uniform film was collected from the autoclave, washed with ultrapure water and absolute ethanol, and dried in compressed N_2 stream. Finally, TiONA grown on the FTO substrate was annealed at 450 °C for 3 h at a heating rate of 5 °C/min.

2.4. Preparation of $MgIn_2S_4$-TiONA heterojunction

$MgIn_2S_4$-TiONA heterojunction was synthesized with a facile hydrothermal method. Initially, magnesium nitrate hexahydrate (0.1538 g), indium nitrate hydrate (0.3609 g) and ultrapure water (20 mL) were added into a 100 mL Teflon-lined stainless-steel autoclave and stirred for 30 min. After 0.2909 g of L-cysteine was added, the obtained solution was continuously stirred for 20 min. The TiONA modified FTO substrate was then placed on the bottom of the autoclave to hydrothermally react at 160 °C for 12 h, and the modified FTO substrate was collected after the autoclave was cooled to room temperature. Finally, it was washed with ultrapure water and dried under a stream of N_2.

2.5. Fabrication of ATP aptasensor

Firstly, 20 μL of aqueous solution of 3-mercaptopropionic acid (MPA, 10 mM) was incubated on $MgIn_2S_4$-TiONA|FTO at 4 °C for 2 h, and the excess MPA was removed by washing with PBS (pH 7.4). Subsequently, the modified FTO electrode was immersed in a solution containing 10 mM 1-ethyl-3-(3-dimethylaminopropyl)carbodiimide (EDC) and 20 mM N-hydroxysuccinimide (NHS) for 30 min at room temperature, and then rinsed with PBS. Next, 20 μL of DNA_1 solution (1 μM) was incubated on the electrode surface for 4 h at 4 °C to conjugate DNA_1 to the modified electrode through an amino coupling reaction between the –COOH group of MPA and the $–NH_2$ group of DNA_1. The electrode was subsequently rinsed for three times with PBS to remove the excess DNA_1 and then blocked by 3% (w/v) BSA solution for 0.5 h to block the remaining active sites. After the excess BSA was washed with PBS, DNA_1|$MgIn_2S_4$-TiONA|FTO was incubated with a sample solution (20 μL) containing increasing concentration of ATP in the presence of signal DNA_2 solution (1 μM) for 1 h, and then thoroughly washed with PBS to minimize non-specific binding and achieve an optimal signal to background ratio.

3. Results and discussion

3.1. Photocurrent generation mechanism of PEC aptasensor

The PEC aptasensor for ATP was prepared with $MgIn_2S_4$-TiONA nanocomposite. Its photocurrent generation mechanism was displayed in Scheme 1. The energy levels of both conduction band (CB) and valence band (VB) of $MgIn_2S_4$ are higher than their counterparts of TiONA, thus the photo-generated electrons could be transferred from the CB of $MgIn_2S_4$ to that of TiONA, and the photogenerated holes were transferred from the VB of TiONA to that of $MgIn_2S_4$, which led to the formation of the electron-hole couples. As a result, the electron donor, ferrocene, labeled to DNA_2 was oxidized by photo-generated holes from Fe^{2+} to Fe^{3+} ($h^+ + Fe^{2+} \rightarrow Fe^{3+}$), which promoted efficient separation of electron-hole pairs, and thus enhanced the photocurrent. Upon the increase of ATP on aptasensor surface, the amount of DNA_2-Fc increased, leading to the increased photocurrent.

3.2. Microscopic characterization of nanomaterials

The size and morphology of the prepared nanomaterials were characterized using the scanning electron microscope. From the plan and side views of bare TiONA (Fig. 1A and B), it could be seen that the aligned array of TiO_2 nanowires with a rectangular cross section was deposited on the FTO substrate to form a uniform film. The diameter of these nanowires was estimated to be from 150 nm to 200 nm, and their average length was approximately 2 μm. Meanwhile, pristine $MgIn_2S_4$ samples (Fig. 1C) were composed of numerous nanoplates with a few micrometers in size because they were severely self-aggregated in the absence of other nanomaterials. The SEM images of $MgIn_2S_4$-TiONA at different magnifications indicated the dense coverage of TiONA surface by the intertwined nanoplates of $MgIn_2S_4$ (Fig. 1D and E), which produced a flower-like heterostructure. Moreover, the side view of the $MgIn_2S_4$-TiONA nanocomposite (Fig. 1F) indicated that TiONAs were tightly bound by $MgIn_2S_4$ nanoplates, further demonstrating the successful preparation of the nanocomposite.

3.3. XPS characterization of the nanomaterials

The surface chemical composition and electronic state of $MgIn_2S_4$-TiONA heterostructure was studied with XPS. The survey spectrum of the heterostructure (Fig. 2A) displayed C 1s, Mg 1s, In 3d and S 2p

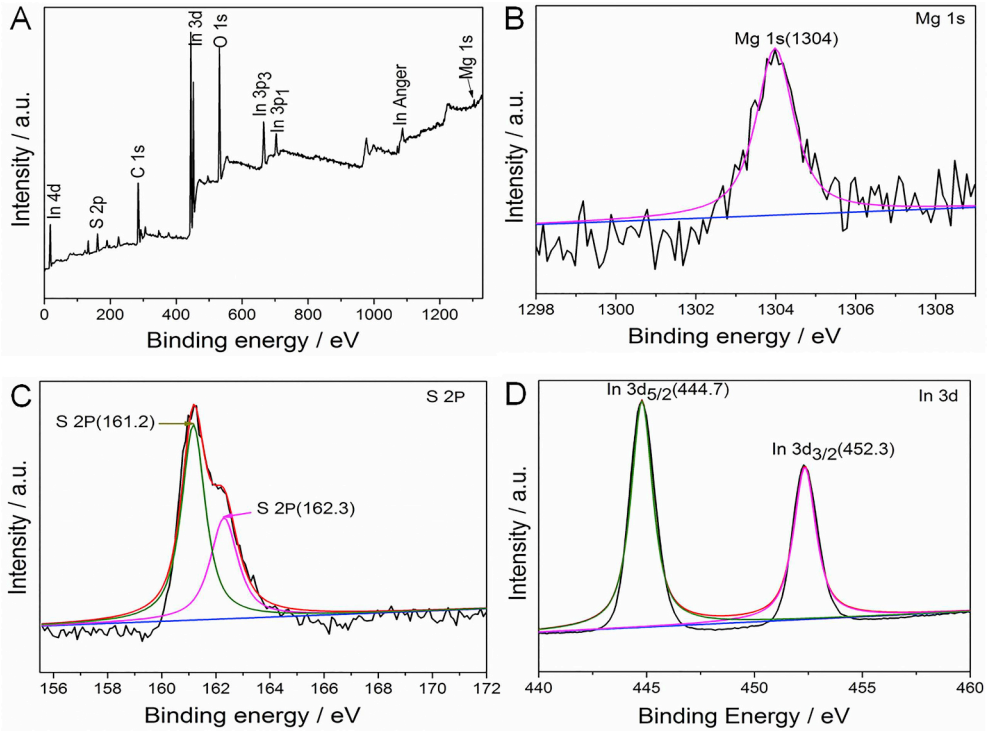

Fig. 2. XPS analysis of $MgIn_2S_4$-TiONA: (A) survey scan, and high resolution spectra of (B) Mg 1s, (C) S 2p, (D) In 3d.

peaks, confirming the successful preparation. The C 1s peak was derived from carbon dioxide adsorbed on the sample surface, and was usually used to make corrections at 284.8 eV. The high resolution spectrum of Mg 1s showed a peak at ~1304 eV (Fig. 2B), which was attributed to the Mg^{2+} oxidation state in $MgIn_2S_4$ nanoplates (Chen et al., 2017b). The S 2p peak was split into two peaks at ~161.2 eV and 162.3 eV (Fig. 2C), corresponding to the binding energy of S^{2-} (Chen et al., 2017a; Di et al., 2016). The high resolution spectrum of In 3d showed two peaks at ~444.7 and 452.3 eV (Fig. 2D), ascribed to the two binding energy of In^{3+} species of In $3d_{5/2}$ and In $3d_{3/2}$ respectively (Chen et al., 2017a). These results indicated that the valence states of Mg, In, S in the composite were ascribed to Mg^{2+}, In^{3+} and S^{2-}.

3.4. XRD and UV–vis diffuse reflectance spectra of the nanomaterials

The crystal structures of the prepared nanomaterials were characterized by X-ray powder diffraction, as shown in Fig. 3A. The XRD pattern of bare FTO substrate (curve a) showed several diffraction peaks at ~26.67°, 33.93°, 37.82°, 51.84°, 54.83°,61.75° and 65.63°, which derived from SnO_2 in FTO, and were labeled by asterisks for comparison purpose. The XRD pattern of TiONA (curve b) presented two characteristic diffraction peaks at ~36.1° and 62.7°, revealing that highly oriented TiO_2 rutile (101) and (002) crystal faces were obtained (Li et al., 2013; Liu et al., 2017c). In the XRD pattern of $MgIn_2S_4$-TiONA composite, a series of diffraction peaks at ~23.5°, 27.7°, 33.5°, 48.1°, 56.4°, 59.8°, 70.3° and 77.1° (curve c) attributed to (220), (311), (400), (440), (533), (444), (800), and (751) crystal faces respectively were observed, corresponding to the cubic structure of $MgIn_2S_4$ phase (JCPDS 31-0792). In addition to these peaks, the other diffraction peaks on curve c derived from TiONA and FTO glass substrate, demonstrating successful preparation of $MgIn_2S_4$-TiONA nanocomposite.

The UV–vis diffuse reflectance spectroscopy (DRS) was applied to characterize the optical properties of the obtained nanomaterials (Fig. 3B). The absorption edge of TiONA was observed at ~410 nm (curve a), indicating its poor visible light absorption. However, the absorption edge of pristine $MgIn_2S_4$ nanoplate was located at ~605 nm (curve b), demonstrating its strong absorption in the visible region. According to the Scherer equation: $\lambda = 1240/Eg$ (λ is the absorption edge wavelength) (Liu et al., 2017b), the bandgap of TiO_2 and $MgIn_2S_4$ were calculated to be ~3.02 eV and 2.05 eV, respectively, which were consistent with their absorption spectra. As expected, the absorption edge of curve c moved to ~560 nm, indicating the successful formation of a $MgIn_2S_4$-TiONA heterojunction, which significantly improved the visible light absorption of the modified photoelectrode.

3.5. Characterization of PEC aptasensor

Electrochemical impedance spectroscopy (EIS) is a sensitive method to monitor the change of interface properties during the step-by-step assembly of biosensors. Herein, impedance experiments were performed in 0.1 M KCl solution containing 5 mM $K_3[Fe(CN)_6]|K_4[Fe(CN)_6]$ with the frequency scanned from 100 kHz to 100 mHz at a potential of 0.230 V superimposed by a 5 mV alternating voltage. As shown in Fig. 3C, the Nyquist diagram of $MgIn_2S_4$-TiONA|FTO possessed a much smaller semicircle diameter (curve b) than TiONA|FTO (curve a), implying the smaller electron transfer resistance (*R*et) of $MgIn_2S_4$-TiONA than that of TiONA. This result was probably because the formation of the heterojunction improved the electron transfer of $[Fe(CN)_6]^{3-/4-}$ at the electrode surface. The immobilization of DNA_1 led to a significant increase in *R*et (curve c), due to the steric hindrance of the biomolecules. After the active sites were blocked by BSA, the modified electrode was incubated with DNA_2 solution in the presence of ATP (1 pM) to form a DNA_1-ATP-DNA_2 sandwich complex layer (curve d), resulting in a significant increase of *R*et value. The impedance results demonstrated the continuous immobilization of the different sensor components on the FTO electrode.

Fig.3D showed the photocurrent responses at different modified electrodes under the intermittent visible light illumination. TiONA|FTO (curve a) showed the smallest photocurrent among all the modified electrodes, probably because of the large bandgap of TiO_2 nanowire array and easy recombination of the electron-hole pairs. Contrast to TiONA|FTO, the photocurrent at $MgIn_2S_4$-TiONA|FTO was enhanced by ~6.8 times, attributed to the matching energy levels between $MgIn_2S_4$ nanoplates and TiONA (curve b), which significantly promoted

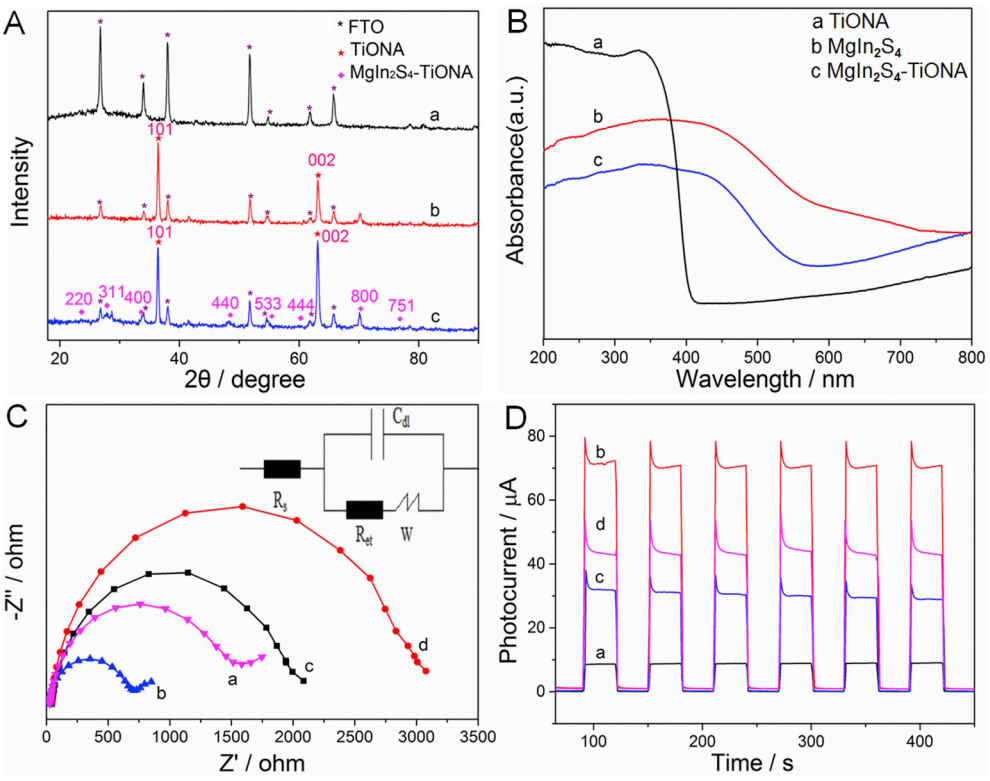

Fig. 3. (A) XRD patterns of (a) FTO substrate, (b) pristine TiONA and (c) $MgIn_2S_4$-TiONA; (B) UV–vis diffuse reflectance spectra of (a) TiONA, (b) $MgIn_2S_4$ and (c) $MgIn_2S_4$-TiONA; (C) EIS of (a) TiONA|FTO, (b) $MgIn_2S_4$-TiONA|FTO, (c) DNA_1|$MgIn_2S_4$-TiONA|FTO, (d) DNA_2-ATP-DNA_1|$MgIn_2S_4$-TiONA|FTO in 0.1 M KCl containing 5 mM $[Fe(CN)_6]^{3-/4-}$; (D) Photocurrent responses of (a) TiONA|FTO, (b) $MgIn_2S_4$-TiONA|FTO, (c) DNA_1-$MgIn_2S_4$-TiONA|FTO and (d) DNA_2-ATP-DNA_1|$MgIn_2S_4$-TiONA|FTO in 0.1 M PBS (pH 7.4) containing 0.1 M KCl at an applied potential of 1 V. The concentrations of both DNA_1 and DNA_2 are 1 μM.

separation of the photo-generated charges. Subsequently, the immobilization of DNA_1 on $MgIn_2S_4$-TiONA|FTO resulted in a photocurrent reduction by ~55% (curve c). This is because the steric hindrance of DNA_1 molecules inhibited the electron transfer at the electrode interface and increased the recombination between electrons and holes. Thereafter, DNA_1-$MgIn_2S_4$-TiONA|FTO was incubated with 20 μL of 1 pM ATP solution and 20 μL of 1 μM ferrocene labeled DNA (DNA_2) solution successively. Both DNA_1 and DNA_2 specifically bound to ATP to form a DNA_1-ATP-DNA_2 sandwich complex, resulting in an increase of photocurrent (curve d). This change could be attributed to the presence of ferrocene, which acted as an electron donor to react with the photo-generated holes, and promote their separation with the electrons (Sui et al., 2018). The above results demonstrated the feasibility of the prepared PEC aptasensor for detection of ATP.

3.6. Optimization of experimental conditions for PEC detection

To achieve the best performance of the PEC aptasensor, the effects of pH and hybridization time on the photocurrent response were optimized. As shown in Fig. 4A, curve a, the photocurrent of the aptasensor rapidly enhanced with the increasing pH of test solution from 5.5 to 7.4, and reached the maximum at pH 7.4. Considering the biological activity of the aptamer, a PBS solution with pH of 7.4 was selected as the detection solution. The photocurrent response of the aptasensor quickly increased with increasing hybridization time and stabilized within 1 h in the presence of 1 pM ATP (Fig. 4A, curve b), indicating the formation of the sandwich complex was equilibrated. Therefore, 1 h was chosen as the best hybridization time for the subsequent test.

3.7. PEC detection of ATP

0.1 μM of ATP was firstly prepared in dimethyl sulfoxide, which was spiked in test solution to obtain different concentrations. Under the optimal conditions, with increasing ATP concentration more DNA_2-Fc were specifically bound to ATP to form the sandwich structure, thus the corresponding photocurrent response was enhanced (Fig. 4B). The photocurrent change ($\Delta I = I - I_0$, where I_0 is the photocurrent in the absence of ATP) was proportional to the logarithm of the ATP concentration from 50 fM to 100 nM (Fig. 4C). A regression equation of $\Delta I = 26.45 + 5.1 \text{ Log } C_{ATP}$ (pM) was obtained with a correlation coefficient of 0.997. The limit of detection was 20 fM, estimated from the calibration plot and the value of average blank signal plus three times standard deviation. Compared with the $MgIn_2S_4$-TiONA heterojunction, the aptasensor prepared with only TiONA on FTO exhibited a much narrower linear range from 10 pM to 1 nM (inset in Fig. 4C) with a detection limit of 9.2 pM due to the poor visible light absorption of TiONA, easy recombination of electron-hole pairs, and the smaller specific surface area of TiONA for loading of biomolecules. As shown in Table S1, the aptasensor based on $MgIn_2S_4$-TiONA heterojunction displayed superiority over most of the previously reported methods such as fluorescence, electrochemistry, colorimetry and chemiluminescence for ATP detection. The improved performance was due to the high specificity and stability provided by the sandwich structure, and the excellent properties of the heterojunction including high photoelectrochemical efficiency, good electrical conductivity and large surface area.

3.8. Specificity, reproducibility and stability of the PEC aptasensor

To assess the specificity of the aptasensor, photocurrent change (ΔI) generated by ATP and some representative interferents including CTP, GTP and UTP were compared under the same conditions. The photocurrent change caused by ATP was at least ~4.5 times larger than those resulted by the other three interferents (Fig. 4D), indicating the negligible interference from these chemicals. The specificity was also evaluated by measuring ΔI in a mixed sample composed of ATP (1 pM), CTP (1 nM), GTP (1 nM) and UTP (1 nM), which showed a response similar to that of 1 pM ATP, revealing the high specificity of the proposed aptasensor for ATP. In addition, the photocurrent change of non-specific DNA-$MgIn_2S_4$-TiONA|FTO to ATP was very small. The reproducibility of the aptasensor was obtained by measuring ATP with six identical sensors prepared under the same experimental conditions. The

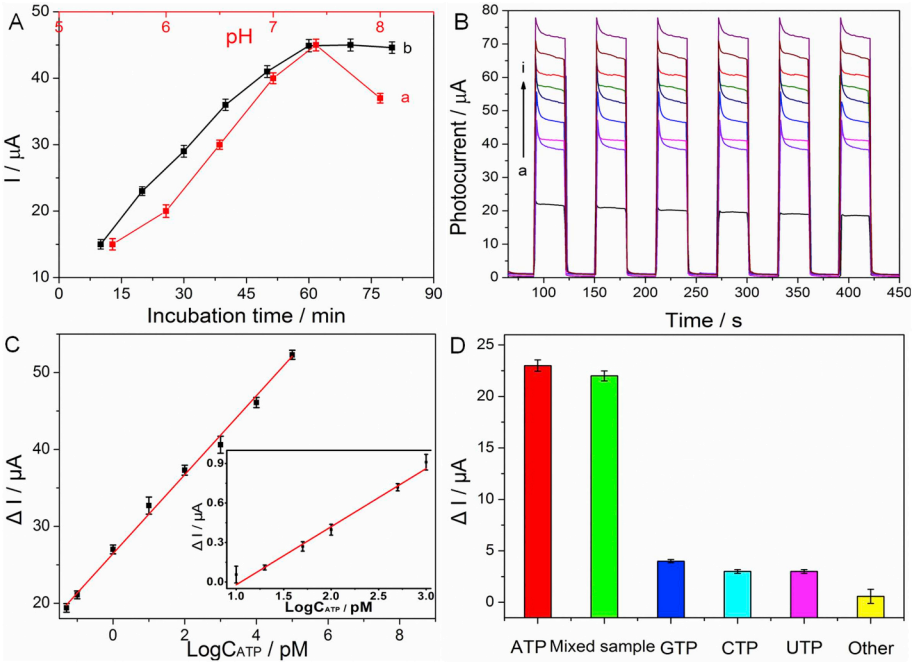

Fig. 4. (A) Effects of pH (a) and incubation time (b) on photocurrent; (B) Photocurrent responses of DNA_1-$MgIn_2S_4$-TiONA|FTO to ATP at 0, 0.05, 0.1, 1, 10, 100, 10^3, 10^4 and 10^5 pM (a to g); (C) Calibration plot of ΔI vs. Log C_{ATP}, Inset: calibration plot of DNA_1-TiONA|FTO at 10, 20, 50, 100, 500 and 1000 pM ATP; (D) Photocurrent changes for 1 pM ATP, 1 nM CTP, 1 nM GTP, 1 nM UTP, and their mixture at DNA_1-$MgIn_2S_4$-TiONA|FTO. The test was performed in 0.1 M PBS (pH 7.4) containing 0.1 M KCl at an applied potential of 1 V. The error bars were derived from the standard deviation of four measurements.

relative standard deviation was calculated to be 4.6%, indicating acceptable repeatability of the aptasensor. To evaluate the long term stability, the PEC aptasensors were placed in a 4 °C refrigerator for 2 weeks and the average photocurrent response maintained ~91.6% of their initial values.

3.9. Real sample analysis using the PEC aptasensor

To verify the feasibility of the designed aptasensor in practical applications, the recoveries of ATP in both blank and real human serum samples were analyzed under the optimal conditions. The spiked samples were prepared by adding different amount of ATP to both blank and real human serum samples. As displayed in Table 1, the recoveries of blank samples varied from 97.8 to 101.4%, and those of real samples were in the range of 95.2–103.6%. The well matched recoveries for the three groups indicated the potential application of the proposed aptasensor in real samples.

4. Conclusion

A novel $MgIn_2S_4$-TiONA heterojunction has been designed as a PEC platform to immobilize biorecognition element for the development of a PEC aptasensor. The heterojunction can be conveniently prepared with a hydrothermal method by growing $MgIn_2S_4$ nanoplates on TiONA. The heterojunction possesses a large surface for loading significant amount of aptamer, excellent biocompatibility and strong absorption efficiency in visible light region. The PEC apatsensor can be constructed by binding capture DNA_1 on the heterostructure, followed by the successive addition of analyte ATP and signal DNA_2 to form a sandwich structure with high selectivity and stability. The PEC aptasensor exhibits a wide linear range along with a detection limit down to 20 fM, high selectivity, good reproducibility and acceptable stability. This work demonstrates that the $MgIn_2S_4$-TiONA heterojunction is an ideal candidate platform to develop PEC biosensing methodology for practical application.

Table 1
Determination of ATP in human serum samples.

Serum sample	Initial	Added	Founded[a]	RSD (%)	Recovery (%)
Blank	0	20 pM	19.6 pM	3.2	97.8
		100 pM	98.4 pM	2.6	98.4
		10 nM	10.1 nM	3.7	101.4
Normal human	51.2 nM	100 pM	49.3 nM	2.6	96.1
		5 nM	53.8 nM	4.2	95.7
		10 nM	59.2 nM	3.1	96.7
Pregnant woman	124.5 nM	100 pM	119.5 nM	3.2	95.9
		5 nM	123.3 nM	2.5	95.2
		10 nM	139.4 nM	4.1	103.6

[a] The results are the average of five determinations.

Declaration of interest statement

The authors declare that they have no known competing financial interests or personal relationships that could have appeared to influence the work reported in this paper.

Credit author statement

This manuscript has not been previously published, and is not currently submitted to any other journal. All authors participated in experiments and/or writing of this manuscript. They have seen and approved the submission of the manuscript. We have no conflicts of interest to disclose.

Acknowledgements

This work was financially supported by National Natural Science Foundation of China (No. U1504215, 21576071, 21776061), International Science and Technology Cooperation Programme funded by The Department of Science and Technology of Henan Province (172102410042), the program for Science & Technology Innovation Talents in Universities of Henan Province (19HASTIT037) and the program for Science & Technology Innovation Team in Universities of Henan Province (19IRTSTHN029).

Appendix A. Supplementary data

Supplementary data to this article can be found online at https://

doi.org/10.1016/j.bios.2019.111487.

References

Cao, J.-T., Zhang, J.-J., Gong, Y., Ruan, X.-J., Liu, Y.-M., Chen, Y.-H., Ren, S.-W., 2015. J. Electroanal. Chem. 759, 46–50.

Chen, T., Song, C., Fan, M., Hong, Y., Hu, B., Yu, L., Shi, W., 2017a. Int. J. Hydrogen Energy 42, 12210–12219.

Chen, W., Hua, Y.-X., Wang, Y., Huang, T., Liu, T.-Y., Liu, X.-H., 2017b. J. Catal. 349, 8–18.

Deng, D., Hao, Y., Yang, S., Han, Q., Liu, L., Xiang, Y., Tu, F., Xia, N., 2019. Sens. Actuators, B 286, 415–420.

Deng, J., Wang, K., Wang, M., Yu, P., Mao, L., 2017. J. Am. Chem. Soc. 139, 5877–5882.

Di, T., Zhu, B., Zhang, J., Cheng, B., Yu, J., 2016. Appl. Surf. Sci. 389, 775–782.

Dong, Y.-X., Cao, J.-T., Liu, Y.-M., Ma, S.-H., 2017. Biosens. Bioelectron. 91, 246–252.

Feng, X., Shankar, K., Varghese, O.K., Paulose, M., Latempa, T.J., Grimes, C.A., 2008. Nano Lett. 8, 3781–3786.

Huo, X., Liu, P., Zhu, J., Liu, X., Ju, H., 2016a. Biosens. Bioelectron. 85, 698–706.

Huo, Y., Qi, L., Lv, X.-J., Lai, T., Zhang, J., Zhang, Z.-Q., 2016b. Biosens. Bioelectron. 78, 315–320.

Jiang, D., Li, J., Xing, C., Zhang, Z., Meng, S., Chen, M., 2015. ACS Appl. Mater. Interfaces 7, 19234–19242.

Kashefi-Kheyrabadi, L., Mehrgardi, M.A., 2012. Biosens. Bioelectron. 37, 94–98.

Li, Y., Yu, H., Zhang, C., Fu, L., Li, G., Shao, Z., Yi, B., 2013. Int. J. Hydrogen Energy 38, 13023–13030.

Liu, P., Huo, X., Tang, Y., Xu, J., Liu, X., Wong, D.K.Y., 2017a. Anal. Chim. Acta 984, 86–95.

Liu, P.P., Liu, X., Huo, X.H., Tang, Y., Xu, J., Ju, H., 2017b. ACS Appl. Mater. Interfaces 9, 27185–27192.

Liu, X., Huo, X., Liu, P., Tang, Y., Xu, J., Ju, H., 2017c. Biosens. Bioelectron. 92, 171–178.

Liu, X., Huo, X., Liu, P., Tang, Y., Xu, J., Liu, X., Zhou, Y., 2017d. Electrochim. Acta 242, 327–336.

Liu, X., Liu, P., Tang, Y., Yang, L., Li, L., Qi, Z., Li, D., Wong, D.K.Y., 2018. Biosens. Bioelectron. 112, 193–201.

Lu, J., Yan, M., Ge, L., Ge, S., Wang, S., Yan, J., Yu, J., 2013. Biosens. Bioelectron. 47, 271–277.

Lu, L., Si, J.C., Gao, Z.F., Zhang, Y., Lei, J.L., Luo, H.Q., Li, N.B., 2015. Biosens. Bioelectron. 63, 14–20.

Murphy, A.B., Barnes, P.R.F., Randeniya, L.K., Plumb, I.C., Grey, I.E., Horne, M.D., Glasscock, J.A., 2006. Int. J. Hydrogen Energy 31, 1999–2017.

Ranjbar, S., Shahrokhian, S., Nurmohammadi, F., 2018. Sens. Actuators, B 255, 1536–1544.

Shahdost-fard, F., Salimi, A., Khezrian, S., 2014. Biosens. Bioelectron. 53, 355–362.

Shahdost-fard, F., Salimi, A., Sharifi, E., Korani, A., 2013. Biosens. Bioelectron. 48, 100–107.

Sui, C., Zhou, Y., Wang, M., Yin, H., Wang, P., Ai, S., 2018. Sens. Actuators, B 266, 514–521.

Tang, Y., Chai, Y., Liu, X., Li, L., Yang, L., Liu, P., Zhou, Y., Ju, H., Cheng, Y., 2018. Biosens. Bioelectron. 117, 224–231.

Verstraeten, L.M.J., De Coninck, K., Vlassak, K., Verstraete, W., Van de Werf, H., Ilaiwi, M., 1983. Soil Biol. Biochem. 15, 397–402.

Wang, B., Cao, J.-T., Dong, Y.-X., Liu, F.-R., Fu, X.-L., Ren, S.-W., Ma, S.-H., Liu, Y.-M., 2018a. Chem. Commun. 54, 806–809.

Wang, D., Xiao, X., Xu, S., Liu, Y., Li, Y., 2018b. Biosens. Bioelectron. 99, 431–437.

Wang, G., Wang, H., Ling, Y., Tang, Y., Yang, X., Fitzmorris, R.C., Wang, C., Zhang, J.Z., Li, Y., 2011. Nano Lett. 11, 3026–3033.

Wang, J., Wang, L., Liu, X., Liang, Z., Song, S., Li, W., Li, G., Fan, C., 2007. Adv. Mater. 19, 3943–3946.

Wu, D., Ren, X., Hu, L., Fan, D., Zheng, Y., Wei, Q., 2015. Biosens. Bioelectron. 74, 391–397.

Xia, N., Chen, Z., Liu, Y., Ren, H., Liu, L., 2017a. Sens. Actuators, B 243, 784–791.

Xia, N., Wang, X., Yu, J., Wu, Y., Cheng, S., Xing, Y., Liu, L., 2017b. Sens. Actuators, B 239, 834–840.

Xu, W., Lu, Y., 2010. Anal. Chem. 82, 574–578.

Yokoshiki, H., Sunagawa, M., Seki, T., Sperelakis, N., 1998. Am. J. Physiol. Cell Physiol. 274, C25–C37.

Yoon, M., Chang, J.A., Kim, Y., Choi, J.R., Kim, K., Lee, S.J., 2001. J. Phys. Chem. B 105, 2539–2545.

Yu, Y., Chen, G., Wang, G., Lv, Z., 2013. Int. J. Hydrogen Energy 38, 1278–1285.

Zhao, L., Wei, Q., Wu, H., Dou, J., Li, H., 2014. Biosens. Bioelectron. 59, 75–80.

Zhou, S.-S., Zhang, L., Cai, Q.-Y., Dong, Z.-Z., Geng, X., Ge, J., Li, Z.-H., 2016. Anal. Bioanal. Chem. 408, 6711–6717.

Zuo, X., Xiao, Y., Plaxco, K.W., 2009. J. Am. Chem. Soc. 131, 6944–6945.